

Counting the uncountable: deep semantic density estimation from Space

Andres C. Rodriguez^[0000–0002–7446–5690] and Jan D. Wegner^[0000–0002–0290–6901]

ETH Zurich, Stefano-francini-platz 5 8093 Zurich, Switzerland
 {andres.rodriguez, jan.wegner}@geod.baug.ethz.ch

Accepted at GCPR 2018

Abstract. We propose a new method to count objects of specific categories that are significantly smaller than the ground sampling distance of a satellite image. This task is hard due to the cluttered nature of scenes where different object categories occur. Target objects can be partially occluded, vary in appearance within the same class and look alike to different categories. Since traditional object detection is infeasible due to the small size of objects with respect to the pixel size, we cast object counting as a density estimation problem. To distinguish objects of different classes, our approach combines density estimation with semantic segmentation in an end-to-end learnable convolutional neural network (CNN). Experiments show that deep semantic density estimation can robustly count objects of various classes in cluttered scenes. Experiments also suggest that we need specific CNN architectures in remote sensing instead of blindly applying existing ones from computer vision.

Keywords: Remote Sensing · Computer Vision · Density Estimation · Deep Learning

1 Introduction

We propose deep semantic density estimation for objects of sub-pixel size in satellite images. Satellite image interpretation is a challenging but very relevant research topic in remote sensing, ecology, agriculture, economics, and cartographic mapping. Since the launch of the Sentinel-2 satellite configuration of the European Space Agency (ESA) in 2015, anyone can download multi-spectral images of up to 10 meter ground sampling distance (GSD) for free. At the same time, Sentinel-2 offers high revisit frequency delivering an image of the same spot on earth roughly every 5 days. However, for applications that need more high-resolution evidence like detecting and counting objects (e.g, supply chain management, financial industry), spatial resolution is too poor to apply traditional object detectors. In this work, we thus propose to circumnavigate explicit object detection by turning the counting problem into a density estimation task. Furthermore, we add semantic segmentation to be able to count objects of very

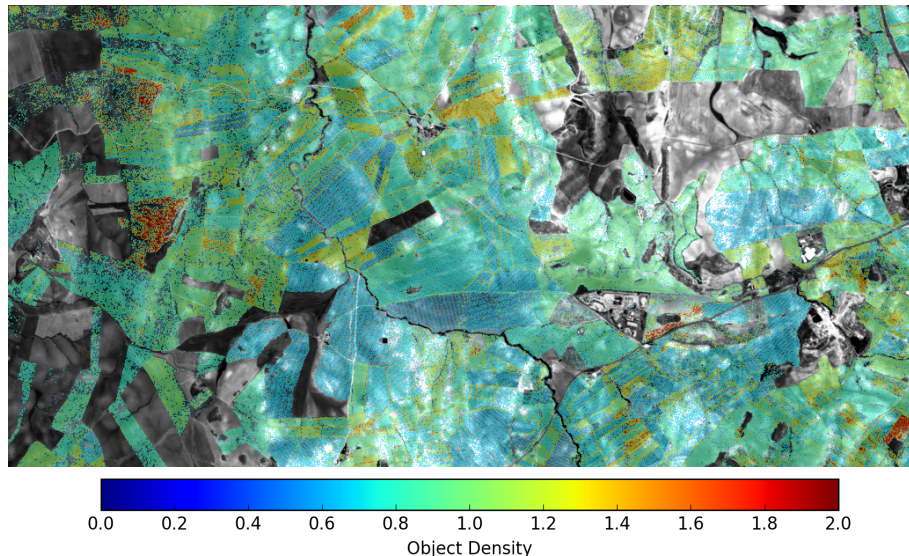


Fig. 1: Density of Olive oil trees in Jaén, Spain, overlaid to a greyscale version of the aerial image. Densities below 0.5 were trimmed for visualization.

specific object categories embedded in cluttered background. We integrate semantic segmentation and density estimation into one concise, end-to-end learnable deep convolutional neural network (CNN) to count objects of $1/3$ the size of the GSD. Semantic Segmentation is a standard task in computer vision and has seen significant performance gains since the comeback of deep learning. The major goal is predicting a class label per pixel over an entire image. A rich set of benchmark challenges and datasets like Cityscapes [6] and Pascal VOC 2012 [8] help making rapid progress in this field while continuously reporting current state-of-the-art in online rankings. Typical objects classes of interest are buildings, persons and vehicles that are (i) clearly visible in the image, (ii) large in size (usually several hundreds of pixels) (iii) and can be distinguished from background and further classes primarily relying on shape and RGB texture. Much of this can be transferred with minor adaptations to overhead imagery of $< 2m$ GSD acquired by drones, aerial sensors, and very high-resolution spaceborne platforms [20,21,25,12]¹. In contrast, objects like cars, trees, and buildings constitute a single pixel or less in remote sensing imagery of Sentinel-2 (10m GSD) and Landsat (40m GSD). While this resolution is sufficient for semantic segmentation of large, homogeneous regions like crops [30,26], counting individual object instances in cluttered background becomes hard. Here, high spectral resolution comes to the rescue. Deep learning techniques can greatly benefit from high spectral resolution that conveys object information invisible to human sight.

¹ see the ISPRS semantic labeling benchmark for an overview <http://www2.isprs.org/commissions/comm3/wg4/results.html>

It can learn complex relations between spectral bands to identify object-specific spectral signatures that support pixel-accurate semantic segmentation.

Our workflow goes as follows: We manually annotate a small sample of the object class of interest in Google Earth aerial images. Large-scale groundtruth is obtained by training Faster R-CNN [27] and then predicting for thousands of object instances. Object detections are manually cleansed and turned into smooth density estimates by filtering with a smoothing kernel. An example for groundtruth of olive tree density is given in Fig.1, where we plot the density obtained from high-resolution aerial images. This reference is used to train, validate, and test our deep semantic density estimation model using Sentinel-2 images. It turns out that deep semantic density estimation can robustly count specific object instances of size well below the GSD by making use of both, spatial texture and spectral signature. We demonstrate that our method robustly scales to $> 200km^2$ counting > 1.6 Mio. object instances.

Our main contributions are: (1) We introduce end-to-end learnable deep semantic density estimation for objects of sub-pixel size, (2) we provide a simplified network architecture that takes advantage of low spatial but high spectral image resolution, (3) we show that standard network architectures from computer vision are inappropriate for this task, and (4) we provide a new, large-scale dataset for object counting in satellite images of moderate resolution.

2 Related Work

There is ample literature for semantic segmentation and object detection in both, computer vision and remote sensing. A full review is beyond the scope of this paper and the reader is referred to top-scoring submissions of benchmarks like Cityscapes [6], MSCOCO [14], and the ISPRS semantic labeling challenge.

Semantic Segmentation has seen significant progress since the invention of fully convolutional neural networks (FCN) [18]. Various improvements to the original architecture have been proposed. For example, more complex Encoder-Decoder models learn features in a lower-dimensional representation and then upscale to the original resolution using deconvolutional layers, making use of middle layer representations or bilinear interpolation [29,2,13,24]. Further ideas include atrous convolutions to prevent lowering the resolution of the learned features and keeping a large receptive field [3,4,5]. Other approaches are based on pyramid pooling where features are learned in different resolutions and then merged in different ways to deal with objects of different sizes and scales [4,5,16].

Object Detection is related to semantic segmentation. Instead of assigning one class label per pixel, its objective is detecting all instances of a specified object class in an image. This translates to automatically drawing bounding boxes around objects but leaving background unlabeled. One of the most widely used deep learning detectors is Faster R-CNN [27], which extracts scale-invariant features for object proposals. Other approaches compute features for different

scales and extract the most relevant scale-features [15]. A more sophisticated variant of object detection is instance segmentation, which adds detailed per-pixel boundaries per object. Today’s quasi gold standard is Mask R-CNN [9] that builds on Faster R-CNN and adds a dense feature map to predict instance boundaries.

Density Estimation is about predicting the local distribution of objects without explicitly detecting them. It is a good option in cases where actual objects cannot be clearly identified due to low spatial image resolution, occlusions etc. One application scenario in computer vision is crowd analysis, where ground level images or image sequences from surveillance cameras are used to estimate the number of people [22,31]. An interesting strategy to ease the learning procedure are ranking operations [17] for density estimation. See [1] for a complete review of crowd counting and density estimation. In remote sensing, density estimation has been used for a variety of applications. [7,28] use deep learning to estimate population density using satellite imagery across large regions. Similarly, [32] estimate densities of buildings in cities with support vector regression and a rich set of texture features. More closely related to our work, [11] estimate forest canopy density from Landsat images, whereas [23] estimate biomass density in wetlands from Worldview-2 imagery. These methods inspire our research because they demonstrate that satellite imagery can be used for density estimates of objects with sizes significantly below the GSD. However, all methods have in common that they compute densities of objects that are densely populating the respective image without (much) clutter. In contrast, we propose fine-grained, species-specific density estimates in scenes where the target class could be one out of many. To the best of our knowledge, we are the first to couple fine-grained semantic segmentation with density estimation for cluttered scenes in satellite images. Moreover, we formulate our method as an end-to-end learnable CNN that learns all features for semantics and density estimation simultaneously from the data.

3 Methods

In this section we describe the technical approach. One problem with basically unrecognizable objects in satellite images is manual annotation of reference data. It is impossible to manually segment individual trees or cars in the Sentinel-2 images of 10 meters GSD. We thus resort to Google Maps overhead images of much higher resolution for groundtruth labeling.

Ground Truth We apply the Faster R-CNN Object detector [27] to very high-resolution (1m GSD) Google Maps images to identify and count reference objects. The detector is tuned to achieve high recall to then manually remove false positive predictions. This allows us to obtain a highly detailed count per area that is used as ground truth to test our model on lower resolution satellite imagery. To down-sample our ground truth to a 10m resolution image, we apply

a Gaussian kernel with a $\sigma = K/\pi$, where K is the down-scale ratio between the high resolution Google Maps images and the lower resolution satellite image (we chose $K = 10$). We compute the mean over a window of $K \times K$ pixels to obtain the sub-sampled ground truth. The semantic segmentation label is obtained by thresholding densities with a score above 0.5 as object class, and as background otherwise. Note that we use only cloud-free Sentinel-2 images that are closest to the sensing date of the high resolution imagery in Google Maps. Most Sentinel-2 bands have larger GSD than 10m and we thus need to resample them. We upscale the 20m GSD bands (B5, B6, B7, B8, B10, B11) to 10m using bilinear interpolation. 60m bands were not used in our experiments due to their low resolution and the low information they convey for vegetation datasets.

Semantic Segmentation and Density Estimation Although semantic segmentation and density estimation are different tasks, they are related and can benefit each other. For mutual, fruitful cooperation of both tasks, we set up a joint training procedure such that most features can be used for either of the goals. Adding the semantic segmentation to density estimation also allows to compute classification metrics from standard semantic segmentation literature. Our approach consists of using ResNet blocks, which contain mainly convolutional layers, to obtain features from the input image. Then, for each task, we add an independent convolutional layer at the end of each architecture. For all training experiments, our Loss is defined as:

$$Loss = \underbrace{CrossEntropy(y_{label}, \hat{y}_{label})}_{L_{semantic}} + \underbrace{(y_{density} - \hat{y}_{density})^2}_{L_{density}} \quad (1)$$

where \hat{y} is the predicted estimate for each task. We test four different network architectures in our experiments to verify which provides the best basis for our approach. We begin with the DeepLab V2 (*DL2*) architecture [3], which uses atrous convolutions to obtain filters that have a larger receptive field. These convolutions, inspired from signal processing “à-trous algorithm” [19], have filters that are dilated with zeros to increase the spatial view of a filter without increasing the number of parameters. Moreover, we experiment with the updated version DeepLab V3 (*DL3*) [4], where pyramid pooling with several atrous convolution filters is implemented. Note that this method is a top performing architecture for semantic segmentation on Cityscapes and PASCAL VOC 2012 datasets, and can therefore be viewed as state-of-the-art in semantic image segmentation. Our third architecture (*Ours*) consists of a simplified 6 Layers ResNet [10] where our fourth variant (*Ours Atrous*) adds a last layer of atrous convolutions.

For both simplified ResNet architectures (*Ours* and *Ours Atrous*) we change all striding operations to 1 and use 6 consecutive ResNet Blocks (Fig. 2). Our method moves away from lower dimensional representations but instead keeps details. 6 layers showed a good performance where deeper networks only had marginal to insignificant improvements at a much higher computational cost. The original architecture was designed for typical computer vision images with few, relatively large objects (> 100 pixels per object) per image. In our case,

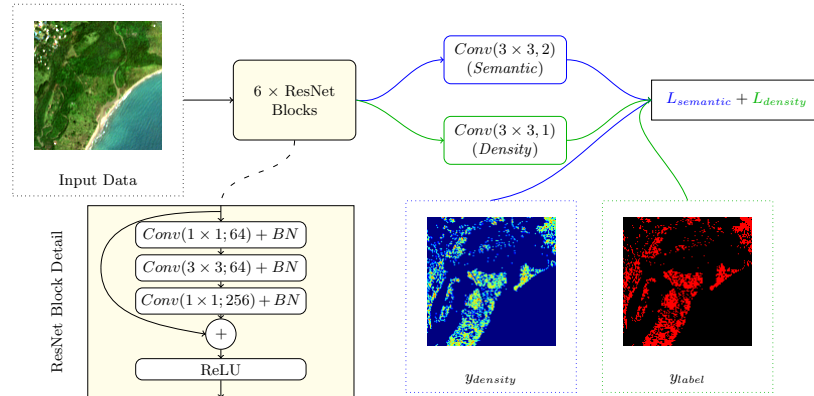


Fig. 2: *Ours* architecture: $Conv(n \times n, M)$ convolution with M filters of size $n \times n$. BN : batch normalization. Input data is first passed through a $Conv(3 \times 3, 256) + BN$ layer before being fed to the first ResNetBlock. Blue and green colors indicate semantic and density connections, respectively. For *Ours Atrous*, all convolutions of the last block before the loss are changed to atrous convolutions.

thousands of object instances of sub-pixel size are present in the image. We want to retain as many details as possible and therefore set stride to 1. We compensate the potential increase in parameters by reducing the size of the receptive field. In fact, we can tolerate learning contextual knowledge within smaller neighborhoods because it is less important in our case.

4 Experiments

In order to test how robust deep semantic density estimation is to changes in texture, object density and size, we create four different datasets. Three datasets contain trees (olive, coconut, oil palm) with different planting patterns and one dataset contains cars². A summary of all datasets is given in Table 1. Note that object sizes range between $1/3$ and $1/4$ of a Sentinel-2 pixel (Ratio Areas). Object densities of the tree datasets are around 1, whereas the car dataset has highest object density (> 5 cars per pixel on average) and smallest object size. Our semi-automated groundtruth annotation procedure involving Faster R-CNN allows us to massively extend our label set across large regions to $> 200km^2$ with > 1.6 Mio. object instances in total (Tab. 1). We validate outcomes of Faster R-CNN predictions on small, manually labeled hold out regions. Intersection over Union (IoU) ranges between 0.82 and 0.97 for Coconut and Olives, respectively. We achieve highest recall for cars (0.92) and lowest for coconut (0.77).

² Cars are reacquired VW Diesels sitting in a desert graveyard at the Southern California Logistics Airport in Victorville, USA.

Dataset	Area (km^2)	Object Count	Object Density ^a	Ratio Areas ^b
Coconuts	77.9	258.7×10^3	0.97	0.36
Palm	104.6	537.5×10^3	1.16	0.36
Olives	129.0	853.7×10^3	0.90	0.39
Cars	0.8	18.3×10^3	5.36	0.26

Table 1: Datasets: ^aMean object density per pixel excluding object free pixels.^bRatio areas = $Area_{Object}/Area_{Pixel}$

Semantic Segmentation and Density Estimation Results of deep semantic density estimation for all architectures are presented in Table 2 and absolute numbers of object counts are shown in Table 3. A visual comparison of ground truth and predictions in Figs. 3 & 4 and the respective χ^2 distance between ground truth distribution $y_{density}$ and predicted distribution $\hat{y}_{density}$ (Table 2, right column) show good performance. *Ours* and *Ours atrous* architectures outperform standard computer vision architectures that build in many downsampling (and upsampling) steps in their network. Results for cars show that there is a natural limitation of our method in terms of minimum object size and maximum object density. While cars can be identified very well (high *IoU*), there exact number is much harder to estimate (higher *MSE*, *MAE* compared to the tree datasets). Moreover, *MSE* is significantly higher than the *MAE*, which is caused by outliers in high density areas where lower densities are erroneously predicted (Fig. 4). Our method seems to have a slight tendency to underestimate high density areas that are surrounded by regions of much lower density. This shortcoming of our method can be observed if comparing ground truth high density areas of olives (red) with the respective, underestimated predictions in the middle row of Figure 3. This effect translates to slightly underestimating the number of instances globally by $< 5\%$ for all datasets (cf.Tab. 3).

Comparison of architectures Our simple architectures *Ours* and *Ours Atrous* consistently outperform *DL2* and *DL3*. *DL2* and *DL3* use strided convolutions to learn lower dimensional representations of the image, which generates higher level features over large areas to learn context. This seems less important in cases where the extent of individual objects in the image is small compared to the pixel size. In fact, strided convolutions and forcing the network to learn lower dimensional representations risks losing high frequency information in the satellite images. We compare activation maps of architectures *DL2* and *Ours* on the coconut dataset in Fig. 5 to visualize this argument. One can observe that filters learned by *DL2* loose details (Fig. 5(a)) required for a fine-grained density prediction in contrast to *Ours* (Fig. 5(b)). Recall that both, *DL2* and *DL3*, use bicubic upsampling at different rates to obtain predictions at the original scale. By removing strided convolutions in our architectures, we avoid the need for upscaling predictions already from the start.

Object	Architecture	Semantic Segmentation			Density			
		IoU	Precision	Recall	MSE	MAE	χ^2 Distance	
Coconut	DL2	0.459	0.673	0.591	0.191	0.355	69.7×10^3	
	DL3	0.528	0.645	0.744	0.168	0.341	62.5×10^3	
	Ours	0.625	0.775	0.763	0.126	0.265	50.6×10^3	
	Ours Atrous	0.649	0.756	0.821	0.122	0.273	81.6×10^3	
Palm	DL2	0.565	0.710	0.734	0.307	0.421	93.8×10^3	
	DL3	0.580	0.694	0.779	0.276	0.415	88.6×10^3	
	Ours	0.660	0.795	0.796	0.192	0.314	75.8×10^3	
	Ours Atrous	0.542	0.544	0.993	0.672	0.668	97.1×10^3	
Olives	DL2	0.777	0.921	0.833	0.235	0.363	30.9×10^3	
	DL3	0.811	0.883	0.909	0.175	0.331	35.6×10^3	
	Ours	0.861	0.901	0.952	0.135	0.270	34.5×10^3	
	Ours Atrous	0.858	0.893	0.957	0.162	0.302	46.5×10^3	
Cars	DL2	0.789	0.928	0.841	8.743	2.235	21.3×10^1	
	DL3	0.753	0.892	0.829	8.454	2.319	25.1×10^1	
	Ours	0.931	0.936	0.994	2.319	1.077	1.6×10^1	
	Ours Atrous	0.941	0.944	0.996	1.940	0.991	3.8×10^1	

Table 2: Semantic Segmentation and Density Estimation over test areas. In **bold** the best performing metric per object class. χ^2 Distance is the histogram distance between ground truth $y_{density}$ and predicted $\hat{y}_{density}$

Band importance Sentinel-2 satellites are multi-spectral sensors designed for vegetation monitoring. Spectral signatures of different vegetation types and plant species can help distinguishing objects, in contrast to mostly texture-based features in RGB images. In order to verify the contribution of this additional spectral evidence, we train and test *Ours Atrous* with different band settings. Each run leaves away bands to test their importance. We contrast results on vegetation with results for cars. We show results of this analysis in Tab. 4, where high *IoU* values of column *Semantic* indicate good identification of objects while low *MSE* and *MAE* values of *Density* mean correct object counting. It turns out that deep semantic density estimation requires both, spectral and spatial evidence for vegetation whereas this is not the case for cars. 10m RGB bands help counting trees (low *MSE* and *MAE* with RGB bands) whereas infrared bands help identifying them (high *IoU* for *All* and *No RGB*). Infrared bands are less important for cars because, unlike plants, they do not reflect characteristic infrared signatures. Prediction is based mostly on texture in the image provided by the 10m RGB bands.

5 Conclusion

We have proposed end-to-end learnable deep semantic density estimation for counting object instances of fine-grained classes in cluttered background. Results

Object	Object Count		
	Ground Truth	Prediction	Diff %
Coconut	88.49×10^3	84.65×10^3	-4.34
Palm	143.14×10^3	137.13×10^3	-4.20
Olives	64.05×10^3	62.34×10^3	-2.68
Cars	4.33×10^3	4.13×10^3	-4.58

Table 3: Object Counting Performance with lowest MSE and MAE error. *Ours* for tree objects and *Ours Atrous* for Cars.

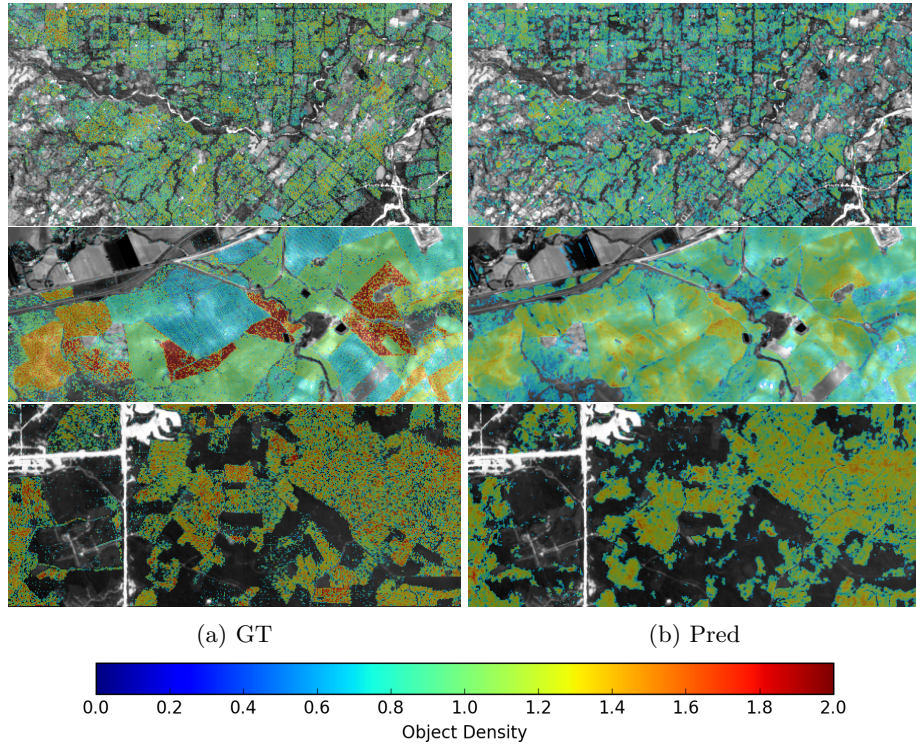


Fig. 3: Density estimation results. Top: Coconut; Middle: Olives; Bottom: Palm. Densities below 0.5 were trimmed for visualization.

show that counting objects of sub-pixel size is possible for 10m GSD satellite images. Experimental evaluation with four datasets shows that our method is robust to change in object types, background, and object density. It turns out that a shallow network specifically designed for satellite imagery of 10m GSD and sub-pixel objects outperforms more sophisticated, state-of-the-art architectures from computer vision. This signifies that direct application of networks tailored for vision to remote sensing images should be done with care. In our

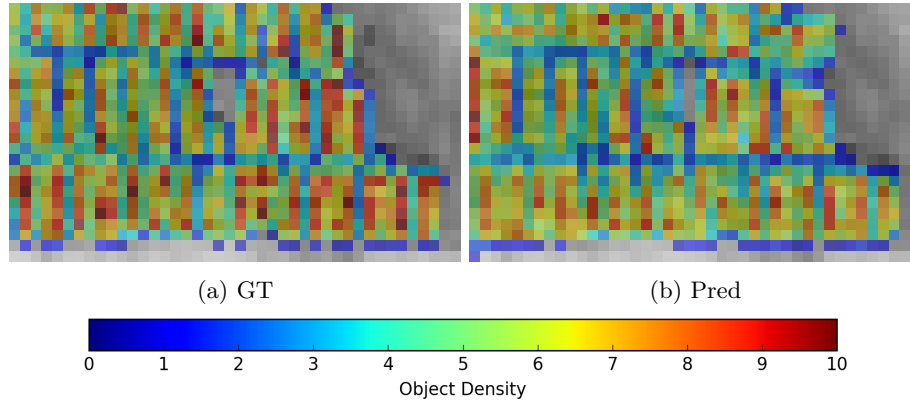


Fig. 4: Car density, densities below 0.5 were trimmed for visualization.

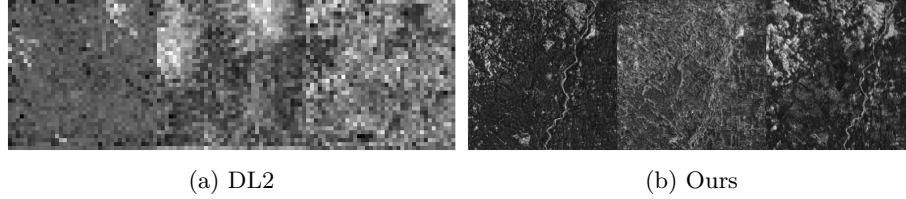


Fig. 5: Final activation maps of (a) *DL2* and (b) *Ours* for a test region of the coconut dataset. *Ours* better retains details than *DL2*.

Bands	Original Pixel Resolution [m]	Coconut			Cars		
		Semantic	Density		Semantic	Density	
		IoU	MSE	MAE	IoU	MSE	MAE
All	10 & 20	0.66	0.13	0.28	0.82	3.56	1.39
RGB	10	0.49	0.26	0.41	0.83	3.53	1.40
RGB I	10	0.55	0.16	0.33	0.77	3.68	1.42
No RGB	10 & 20	0.63	0.19	0.35	0.81	4.45	1.57

Table 4: Band Importance: **top two** per dataset. All: 10m and 20m bands. RGB: B2, B3, B4. RGBI: RGB plus infrared (B8). No RGB: all 10m and 20m bands except RGB.

experiments, we find that any down-sampling operation inside the network risks losing precious details. We should thus always keep in mind the particularities of remote sensing imagery in terms of object scale, GSD, (nadir) perspective and (high) spectral resolution. If carefully considered during the network design process, these specific properties offer new possibilities in network design.

Acknowledgments

This project is funded by Barry Callebaut Sourcing AG as a part of a Research Project Agreement with ETH Zurich.

References

1. A survey of recent advances in cnn-based single image crowd counting and density estimation. *Pattern Recognition Letters* **107**, 3 – 16 (2018), video Surveillance-oriented Biometrics
2. Badrinarayanan, V., Kendall, A., Cipolla, R.: Segnet: A deep convolutional encoder-decoder architecture for image segmentation. *IEEE Transactions on Pattern Analysis and Machine Intelligence* **39**(12), 2481–2495 (2017)
3. Chen, L., Papandreou, G., Kokkinos, I., Murphy, K., Yuille, A.L.: Deeplab: Semantic image segmentation with deep convolutional nets, atrous convolution, and fully connected crfs. *IEEE Transactions on Pattern Analysis & Machine Intelligence* **40**(4), 834–848 (2018)
4. Chen, L., Papandreou, G., Schroff, F., Adam, H.: Rethinking atrous convolution for semantic image segmentation. *CoRR*
5. Chen, L., Zhu, Y., Papandreou, G., Schroff, F., Adam, H.: Encoder-decoder with atrous separable convolution for semantic image segmentation. *CoRR*
6. Cordts, M., Omran, M., Ramos, S., Rehfeld, T., Enzweiler, M., Benenson, R., Franke, U., Roth, S., Schiele, B.: The cityscapes dataset for semantic urban scene understanding. In: *Proc. of the IEEE Conference on Computer Vision and Pattern Recognition (CVPR)* (2016)
7. Doupe, P., Bruzelius, E., Faghmous, J., Ruchman, S.G.: Equitable development through deep learning: The case of sub-national population density estimation. In: *Proceedings of the 7th Annual Symposium on Computing for Development*. p. 6. ACM (2016)
8. Everingham, M., Van Gool, L., Williams, C.K.I., Winn, J., Zisserman, A.: The PASCAL Visual Object Classes Challenge 2012 (VOC2012) Results. <http://www.pascal-network.org/challenges/VOC/voc2012/workshop/index.html>
9. He, K., Gkioxari, G., Dollr, P., Girshick, R.: Mask r-cnn. In: *2017 IEEE International Conference on Computer Vision (ICCV)*. pp. 2980–2988 (2017)
10. He, K., Zhang, X., Ren, S., Sun, J.: Deep Residual Learning for Image Recognition. In: *Proceedings of the IEEE conference on computer vision and pattern recognition*. pp. 770–778 (2016)
11. Joshi, C., De Leeuw, J., Skidmore, A., van Duren, I., van Osten, H.: Remotely sensed estimation of forest canopy density: A comparison of the performance of four methods. *International Journal of Applied Earth Observation and Geoinformation* **8**(2), 84–95 (2006)
12. Kuo, T.S., Tseng, K.S., Yan, J.W., Liu, Y.C., Frank Wang, Y.C.: Deep aggregation net for land cover classification. In: *The IEEE Conference on Computer Vision and Pattern Recognition (CVPR) Workshops* (June 2018)
13. Lin, G., Milan, A., Shen, C., Reid, I.: Refinenet: Multi-path refinement networks for high-resolution semantic segmentation. In: *2017 IEEE Conference on Computer Vision and Pattern Recognition (CVPR)*. vol. 00, pp. 5168–5177 (2017)
14. Lin, T.Y., Maire, M., Belongie, S., Hays, J., Perona, P., Ramanan, D., Dollá, P., Zitnick, C.L.: Microsoft COCO: Common Objects in Context. In: *Proceedings of the European conference on computer vision*. pp. 740–755 (2014)

15. Liu, W., Anguelov, D., Erhan, D., Szegedy, C., Reed, S., Fu, C.Y., Berg, A.C.: Ssd: Single shot multibox detector. In: Leibe, B., Matas, J., Sebe, N., Welling, M. (eds.) *Computer Vision – ECCV 2016*. pp. 21–37. Springer International Publishing, Cham (2016)
16. Liu, W., Rabinovich, A., Berg, A.C.: Parsenet: Looking wider to see better. *CoRR*
17. Liu, X., van de Weijer, J., Bagdanov, A.D.: Leveraging unlabeled data for crowd counting by learning to rank. In: *The IEEE Conference on Computer Vision and Pattern Recognition (CVPR)* (June 2018)
18. Long, J., Shelhamer, E., Darrell, T.: Fully convolutional networks for semantic segmentation. In: *Proceedings of the IEEE conference on computer vision and pattern recognition*. pp. 3431–3440 (2015)
19. Mallat, S.: *A Wavelet Tour of Signal Processing, Third Edition: The Sparse Way*. Academic Press, Inc., Orlando, FL, USA, 3rd edn. (2008)
20. Marmanis, D., Wegner, J.D., Galliani, S., Schindler, K., Datcu, M., Stilla, U.: Semantic segmentation of aerial images with an ensemble of cnns. *ISPRS Annals of the Photogrammetry, Remote Sensing and Spatial Information Sciences* **3**, 473 (2016)
21. Mátyus, G., Luo, W., Urtasun, R.: Deeproadmapper: Extracting road topology from aerial images. In: *International Conference on Computer Vision*. vol. 2 (2017)
22. Meynberg, O., Cui, S., Reinartz, P.: Detection of high-density crowds in aerial images using texture classification. *Remote Sensing* **8**(6), 470 (2016)
23. Mutanga, O., Adam, E., Cho, M.: High density biomass estimation for wetland vegetation using Worldview-2 imagery and random forest regression algorithm. *International Journal of Applied Earth Observation and Geoinformation* **18**, 399–406 (2012)
24. Pohlen, T., Hermans, A., Mathias, M., Leibe, B.: Full-resolution residual networks for semantic segmentation in street scenes. In: *The IEEE Conference on Computer Vision and Pattern Recognition (CVPR)* (July 2017)
25. Postadjan, T., Le Bris, A., Sahbi, H., Mallet, C.: Investigating the potential of deep neural networks for large-scale classification of very high resolution satellite images. *ISPRS Annals of the Photogrammetry, Remote Sensing and Spatial Information Sciences* **4**, 183 (2017)
26. Pryzant, R., Ermon, S., Lobell, D.: Monitoring ethiopian wheat fungus with satellite imagery and deep feature learning. In: *The IEEE Conference on Computer Vision and Pattern Recognition (CVPR) Workshops* (July 2017)
27. Ren, S., He, K., Girshick, R., Sun, J.: Faster r-cnn: Towards real-time object detection with region proposal networks. *IEEE Transactions on Pattern Analysis and Machine Intelligence* **39**(6), 1137–1149 (2017)
28. Robinson, C., Hohman, F., Dilkina, B.: A deep learning approach for population estimation from satellite imagery. In: *Proceedings of the 1st ACM SIGSPATIAL Workshop on Geospatial Humanities*. pp. 47–54. ACM (2017)
29. Ronneberger, O., Fischer, P., Brox, T.: U-net: Convolutional networks for biomedical image segmentation. In: Navab, N., Hornegger, J., Wells, W.M., Frangi, A.F. (eds.) *Medical Image Computing and Computer-Assisted Intervention – MICCAI 2015*. pp. 234–241. Springer International Publishing, Cham (2015)
30. Russwurm, M., Korner, M.: Temporal vegetation modelling using long short-term memory networks for crop identification from medium-resolution multi-spectral satellite images. In: *The IEEE Conference on Computer Vision and Pattern Recognition (CVPR) Workshops* (July 2017)

31. Shang, C., Ai, H., Bai, B.: End-to-end crowd counting via joint learning local and global count. In: 2016 IEEE International Conference on Image Processing (ICIP). pp. 1215–1219 (2016)
32. Zhang, T., Huang, X., Wen, D., Li, J.: Urban Building Density Estimation From High-Resolution Imagery Using Multiple Features and Support Vector Regression. *IEEE Journal of Selected Topics in Applied Earth Observation and Remote Sensing* **10**(7), 3265–3280 (2017)